Polyaniline Based Composite of Non-Covalently Dispersed Multiwalled Carbon Nanotubes for Supercapacitor Electrode

Nabila Nabi Nova[1], Md. Mominul Islam[1], Saika Ahmed[1], M. Muhibur Rahman[1], M. Yousuf A. Mollah[2] and Md. Abu Bin Hasan Susan[1*]
[1]Department of Chemistry, University of Dhaka, Dhaka, Bangladesh. Email: susan@du.ac.bd
[2]University Grants Commission of Bangladesh, 29/1 Agargaon, Sher-E-Banglanagar, Dhaka, Bangladesh.
*Corresponding Author

Abstract: A composite of Multiwalled Carbon Nanotubes (MWCNTs) and polyaniline (PAni) was synthesized by in situ oxidative polymerization of aniline monomers on poly (sodium 4-styrenesulfonate) (PSS) dispersed MWCNTs to produce coaxial structures of MWCNT-PAni composite. The structural, morphological, thermal, surface, and capacitive properties of the composite were analyzed. Scanning electron microscopy images of the composite revealed nanofibrous structure. Infrared spectrum showed slight shifts for several bands of the composite from the bands of PAni to suggest that the MWCNTs have strong attractive interactions with the PAni backbone. The composite was fabricated onto a graphite electrode and the fabricated electrode was characterized using cyclic voltammetry. The fabricated electrode exhibited specific capacitance values of 446 Fg-1, and the value retained 82.5% after 800 cycles. Owing to the good capacitance behavior and cycling stability, the synthesized composite holds promise for energy storage devices like supercapacitors.

Keywords: Carbon nanotube, Non-covalent functionalization, Polyaniline, Supercapacitor.

I. Introduction

For the last two decades since its reported discovery in 1991 by S. Ijima [1], the allotrope under consideration, Carbon Nanotube (CNT), owing to its outstanding mechanical properties, excellent thermal conductivities, and tailorable electrical and chemical properties, has been exploited in a wide range of applications involving nanoscale systems [2]. Due to their large surface area, low resistivity and superior cycle stability, CNTs are excellent materials for use in electrical energy storage devices like supercapacitors. In fact, composites incorporating a CNT backbone coated by an active phase with pseudocapacitive properties, such as CNT/oxide or CNT/polymer composite, represent an important breakthrough for developing a new generation of supercapacitors. These are based on greater effective percolation of electrolyte due to the open mesoporous network of CNTs and the robustness of CNTs which resist volumetric changes during charge-discharge cycles, leading to enhancement of the cycling performance [3].

Polyaniline (PAni), a conducting polymer which conducts electricity by Mott's variable range hopping mechanism of polarons and bipolarons, is an attractive material for use as electrode in supercapacitors because of high specific capacitance, tunable electrical properties by reversible doping and high conductivity in the doped state which takes part in the charging process, fast charge/discharge electro-transfer kinetics and low cost, ease of synthesis, excellent thermal and environmental stability and easy processability due to reversible doping [4-6]. In recent years, the use of CNTs and conducting polymers [7-14] like polyaniline [7-10] in the synthesis of nanocomposites for energy storage applications has substantially attracted the attention of scientists around the globe, on account of electrodes fabricated from such composites exhibiting synergetic effects, for instance, good cycle stability and high capacitance. These factors have greatly enhanced the performances of energy storage devices such as supercapacitors [15].

Supercapacitors have high power densities, but low energy densities. They have been a fascinating choice for the energy storage applications in electric, hybrid electric, and fuel cell vehicles, where they will serve as a short-time energy storage device with high power capability and allow energy storage from regenerative braking [3]. Polymers [16-20], metal oxides [21-25], and their composites [26-29] have been known to exhibit double layer and pseudo-capacitance behaviors. Porous carbon materials such as activated carbon [30,31] and CNTs [32-37] exhibit double-layer capacitance, in addition to pseudocapacitance due to electrochemically active redox reactions [6].

An underlying problem associated with the processing of CNTs prior to the synthesis of nanocomposites is their entanglement.

Carbon nanotubes, due to the strong attractive interactions, namely van der Waals forces and π-π stacking between individual tubes, exist as entangled bundles, as a consequence of which the interfacial interaction between CNTs and polymer matrix is below par when composites are synthesized. This leads to diminished performance of the composite as electrode material [38].

Conventional methods of dispersion include mechanical and covalent dispersions, which are detrimental to the CNT structure and environmentally harmful as well. On the contrary, physical or non-covalent functionalization results in the dispersion of CNTs without damaging their structure or harming the environment, by using polymers and surfactants [39-44] instead of strong acids or vigorous mechanical agitations.

The work aims at synthesizing a composite of Multiwalled Carbon Nanotubes (MWCNTs) and PAni by following an environmentally friendly method of non-covalent functionalization [45] in which MWCNTs was dispersed in PAni using poly (sodium 4-styrenesulfonate) as a dispersant. Structural and compositional characteristics of the composite were compared with MWCNTs and PAni and distinctive features of the nanocomposite were analyzed. Finally, attempts have been made to correlate morphological, topological, and capacitive properties to the structure of the nanocomposite.

II. Experimental

A. Synthesis of MWCNT-PAni Composite and PAni

Multiwalled carbon nanotube (Diameter: 6-9 nm, length: 5 μm; Sigma Aldrich), poly (sodium 4-styrenesulfonate) (PSS, M_W~70,000, Sigma Aldrich), ammonium peroxydisulfate (APS, $(NH_4)_2S_2O_8$, Merck, India) and hydrochloric acid (HCl, RCI Labscan Ltd, Thailand) were used as received and were used for the synthesis of MWCNT-PAni binary composite and PAni without any further purification. Aniline ($C_6H_5NH_2$, Merck, India) was distilled prior to use. All other chemicals were used without further purification. De-ionized water (DI; conductivity: 0.055 μScm^{-1} at 25.0 °C) from HPLC grade water purification systems (BOECO, Germany) was used for the preparation of all aqueous solutions.

The entangled MWCNTs (20 mg) were dispersed by non-covalent functionalization which was carried out by sonication with PSS (0.6 mL 18 wt% solution in DI water) for 30 min. Wrapping of PSS around MWCNT stabilized it by static charge repulsion and the -SO_3^- groups acted as templates for attachment of anilinium ions to the MWCNTs. 7.50 mL of 2 M HCl solution was used for doping 100 μL aniline. 0.5 g APS was dissolved in 25 mL DI water and used as oxidant for the oxidative polymerization of aniline. Aniline to APS mole ratio taken was 1:2.

The MWCNT-PAni composite was synthesized by oxidative polymerization of aniline on PSS dispersed MWCNTs. 100 μL of aniline and aqueous solution of HCl were added to the PSS dispersed MWCNT solution, and sonicated for 10 min. Aqueous solution of APS was added dropwise into the above mixture in an ice bath for 6 h under constant stirring. The prepared MWCNT/PAni composite was left to stand overnight, then collected using centrifugation and washed with acetone, ethanol and DI water, and finally dried at 80 °C for 12 h in vacuum. PAni was synthesized by a similar procedure. In this case, the aniline-HCl mixture was stirred for 2 h in ice bath with dropwise addition of APS until the mixture turned blue-green. The mixture was then left to stand overnight and the PAni was washed and dried as mentioned above.

B. Material Characterization and Electrochemical Analysis

The MWCNT, MWCNT-PAni composite and PAni were characterized using Fourier transform infrared (FTIR) spectroscopy (Frontier FT-IR/NIR, PerkinElmer, USA), scanning electron microscopy (JSM-6490LA, JEOL, Japan), thermogravimetry (Exstar 7200 TG-DTA, Hitachi, Japan), dynamic light scattering (DLS) technique (Zetasizer Nano ZS90, Malvern Instruments Ltd., UK), Brunauer-Emmett-Teller (BET) surface area analyzer (BELSORP mini-II, BEL Japan Inc.) and UV-visible spectroscopy (Spectro UVD-3500, Labomed Inc., USA) to assess their molecular, structural, morphological, and topological properties.

For FTIR spectra measurements, KBr pellets were used. UV-visible absorption spectra were recorded by dispersing the samples in ethanol. Surface area and pore size distribution were determined from adsorption-desorption of N_2 gas at different relative pressures and a constant temperature of -196 ^oC on the surface of MWCNTs, MWCNT-PAni composite, and PAni after pre-treatment. To fabricate the electrode, 3.3 mg of the MWCNT-PAni composite was dispersed with 20 wt % poly(vinyl alcohol) (PVA, M_W~88,000) binder in 200 μL ethanol and 25 μL of this solution was cast onto the surface of a graphite electrode having surface area 1.13 cm^2, which was dried in vacuum at 80 ^oC for 12 h. The fabricated graphite was used as the working electrode for electrochemical measurements. An electrochemical workstation (CHI 760E, CH Instruments Inc., USA) was used for the electrochemical measurements. A three-electrode cell consisting of Ag/AgCl and platinum as reference and counter electrodes, respectively was used for electrochemical analysis. 0.5 M aqueous solution of Na_2SO_4 was used as the electrolyte, which was purged with N_2 gas for 20 min prior to measurements.

III. Results and Discussion

A. Material Characterization

a. *Structural Characterization*

Fig. 1 shows the FTIR spectra of MWCNT, MWCNT-PAni composite, and PAni. The spectrum for pristine MWCNT (Fig. 1a) shows that the band at wavenumber 3452 cm^{-1} is due to O-H stretching vibration on the surface of MWCNTs; this

might have originated either from ambient moisture bound to the MWCNT surface, or some species present in the structure that arose during the purification of the MWCNTs. The band at 1577 cm^{-1} can be attributed to the IR active phonon mode of the MWCNTs [46]. For pristine PAni (Fig. 1c), the bands at 1485 and 1575 cm^{-1} can be assigned to the C-C stretching vibrations of the benzenoid and quinoid rings [47]. Furthermore, the bands at 1312 cm^{-1}, 1415 cm^{-1}, and 3133 cm^{-1} correspond to C-N stretching vibrations of aromatic amines and short-chain oligomers, and C-H stretching vibration, respectively. The N=Q=N stretching band at 1140 cm^{-1} is the characteristic band of polyaniline base; this band was described by Macdiarmid *et al.* as the "electron-like band" and is considered to be a measure of delocalisation of electrons and, thus, it is a characteristic peak of PAni conductivity. The band appearing at 825 cm^{-1} is attributed to an out-of-plane C-H vibration [48].

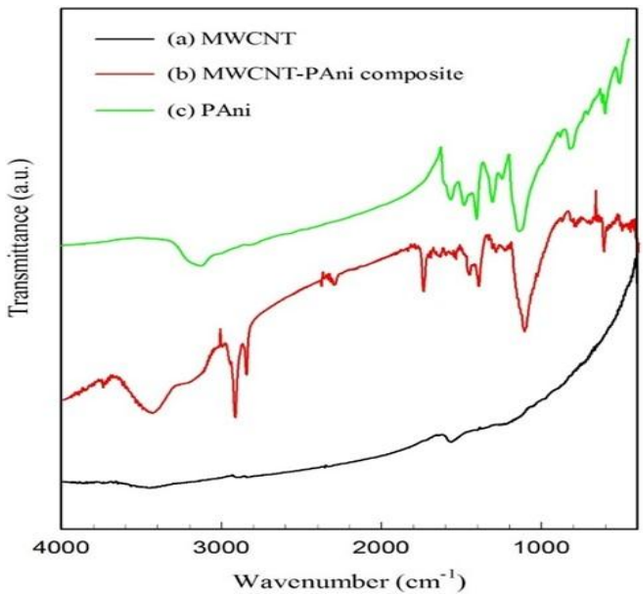

Fig. 1: FTIR Spectra of (a) MWCNT, (b) MWCNT-PAni Composite, and (c) PAni

The spectrum of MWCNT-PAni composite (Fig. 1b) has peaks similar to PAni and MWCNT: at 3440 cm^{-1} (O-H stretching), 2855 and 2930 cm^{-1} (C-H stretching), 1408 and 1115 cm^{-1} (C-N stretching), 1467 cm^{-1} (aromatic C-C stretching). This suggests that the backbone of PAni was not damaged by MWCNTs and that the aniline monomers underwent polymerization on the surface of MWCNTs [47]. In addition, the bands characteristic of PAni shifted to lower wavenumbers, indicating that the MWCNTs exhibited strong attractive interactions with the quinoid units of PAni backbone, hence weakening the bonds within the PAni backbone [49].

b. *UV–visible Spectral Analysis*

The interfacial interaction between PAni and MWCNTs was characterized using UV-visible spectra (Fig. 2). MWCNTs (Fig. 2a) have a strong characteristic absorbance peak at 250 nm, corresponding to additional absorption due to the 1D Van Hove singularities [44]. It can, therefore, be inferred that the CNTs are successfully dispersed in the solvent. PAni (Fig. 2c) and the MWCNT-PAni composite (Fig. 2b) exhibit sharp absorption peaks at 207 and 205 nm, respectively [50], indicating π-π^* transition of the benzenoid ring of the PAni units in both the PAni and the composite via extended conjugation between adjacent rings in the polymeric chains. The peaks of PAni at 246 and 292 nm and those of MWCNT-PAni composite at 235 and 286 nm also correspond to π-π^* transition. PAni has also a weak absorption peak at 376 nm, which can be attributed to polaron-π^* transitions because of cationic species called polarons.

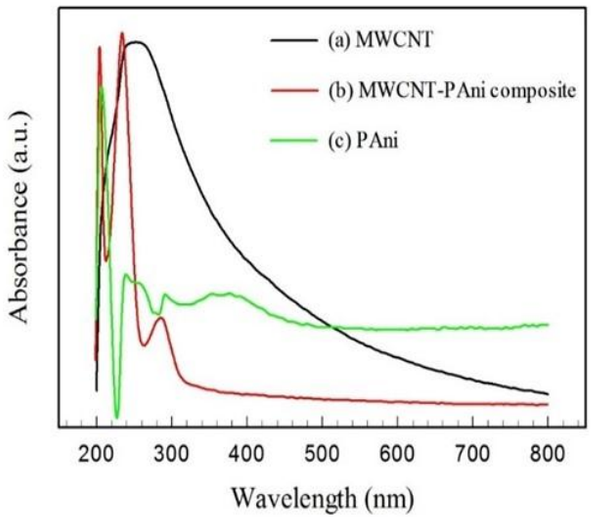

Fig. 2: Absorption Spectra for (a) MWCNT, (b) MWCNT-PAni Composite, and (c) PAni

The hypsochromic shift in the bands for MWCNT-PAni composite as compared to pristine PAni suggests strong interactions between the quinoid rings of the PAni backbone and MWCNTs. Moreover, this indicates that the interaction between CNT and PAni layer facilitates electron delocalization, which enhances the conductivity of the composite [47, 50].

c. *Morphological Analysis*

The morphology of MWCNTs, PAni, and their composite can be interpreted from their SEM images shown in Fig. 3. Fig. 3a shows the SEM image of MWCNTs in which the tubular structure cannot be readily understood. In fact, this is not surprising. Formation of dense agglomerates is apparent due to their entanglement which arises from attractive forces of van der Waals force and π-π stacking between the individual tubes [38]. PAni (Fig. 3c), is in the form of granular, rod-like aggregates, which do not possess clearly defined nanostructure. The SEM image of MWCNT-PAni composite (Fig. 3b), on the other hand, shows coaxial, tubular structure, which is formed by encapsulation of the MWCNTs by PAni.

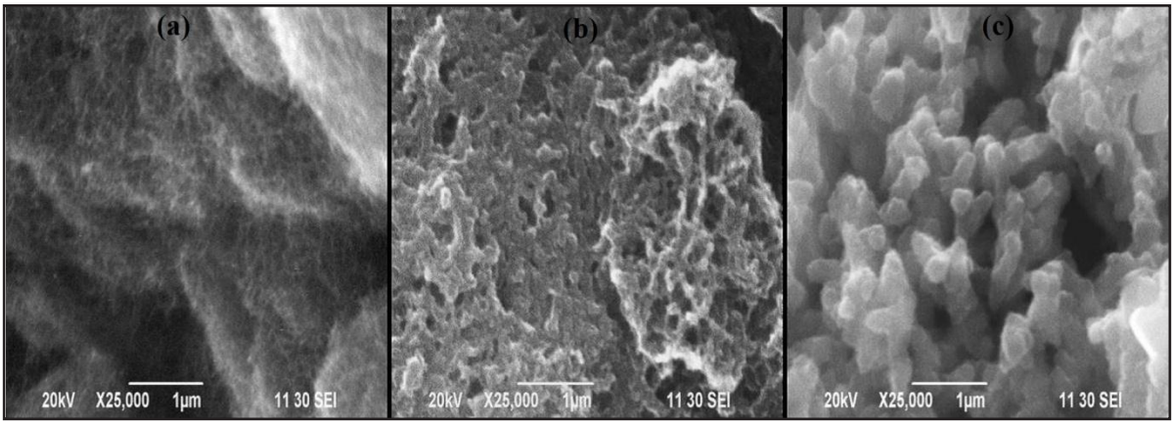

Fig. 3: SEM Images of (a) MWCNT, (b) MWCNT-PAni Composite, and (c) PAni

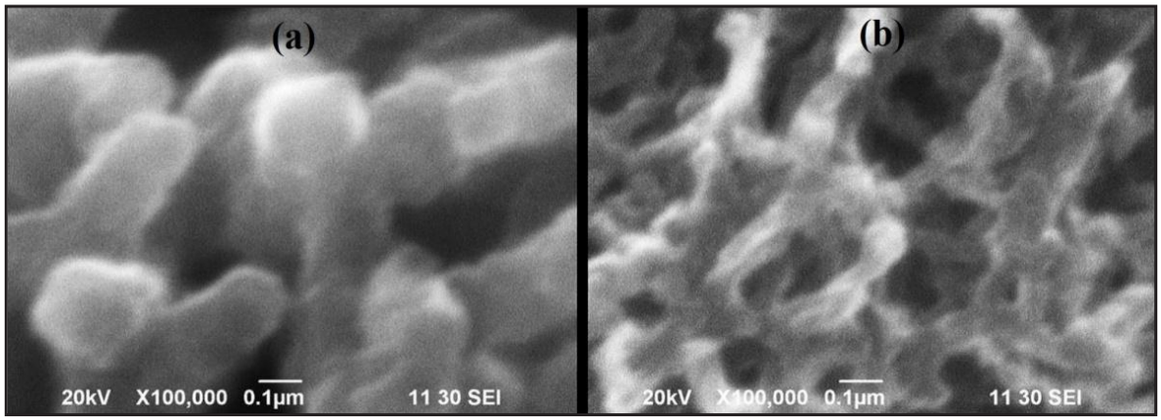

Fig. 4: SEM Images of (a) PAni and (b) MWCNT-PAni Composite

The SEM images of PAni and MWCNT-PAni composite at a higher magnification are shown in Fig. 4. It can be observed that the rod-like aggregates of PAni (Fig. 4a) have diameters from around 100 to 180 nm, the average diameter being ca. 140 nm. The tube-like aggregates of the MWCNT-PAni composite (Fig. 4b), however, have diameters of around 80-90 nm, from which it can be deduced that the MWCNT-PAni composite is in the form of nanofibers, resulting from uniform coating or encapsulation of aniline monomers on the PSS dispersed MWCNTs. Nanofiber structure also suggests that the MWCNTs were well dispersed by PSS before polymerization took place.

d. *Thermal Stability and Compositional Characterization*

Fig. 5 shows thermogravimetric (TG) curves for MWCNT, MWCNT-PAni composite, and PAni under nitrogen atmosphere. The TG curves show that the degree of thermal degradation of MWCNT-PAni composite (Fig. 5b) is lower than that of PAni (Fig. 5c) but higher than that of pristine MWCNTs (Fig. 5a). The initial degradation temperature of PAni is 160 ^{o}C, whereas that of MWCNT-PAni composite is 210 ^{o}C, which suggests that the thermal stability of the composite is greater than that of pristine PAni. The improved thermal stability of the composite in comparison to pristine PAni is due to enhanced van der Waals and π-π interactions between the benzenoid units of the PAni and MWCNTs [47].

The TG curves (Fig. 6) of MWCNT, MWCNT-PAni composite, and PAni under oxygen atmosphere may be compared to determine the composition of MWCNT in the MWCNT-PAni composite. The TG curve of MWCNTs in air (Fig. 6a) shows that MWCNTs are thermally very stable and start to degrade at around 500 °C. The weight loss of about 96% at about 630 °C suggests that the backbone of the CNT structure is entirely broken down. In the thermograms of doped polymers like PAni, the first step loss usually takes place at temperatures below 100 °C, which corresponds to the loss of ambient moisture. The second step loss takes place at temperatures below 250-270 °C, corresponding to the loss of oligomers and dopants. Further mass losses correspond to degradation of the backbone of the polymer [47]. The TG curve of PAni (Fig. 6c) reveals that it contained 3 wt% of ambient moisture, which was lost at temperatures below 100 ^{o}C. A further loss of 17 wt% occurred before reaching a temperature of 260 ^{o}C, due to the loss of dopant and oligomers. The mass losses above this temperature can be attributed to the degradation of the PAni backbone, with the highest amount of degradation occurring between 250 and 320 °C. The TG curve of MWCNT-PAni composite (Fig. 6b)

shows the following mass losses: ambient moisture- 5 wt% (below 100 ^{o}C), dopant and oligomers- 5 wt% (below 270 °C). In this case, the degradation and decomposition of the backbone took place between 270 and 660 ^{o}C. Hence, it can be inferred that the thermal stability of the polymer chains of PAni is enhanced due to incorporation of MWCNTs in the structure. This supports the data from the TG studies under nitrogen atmosphere.

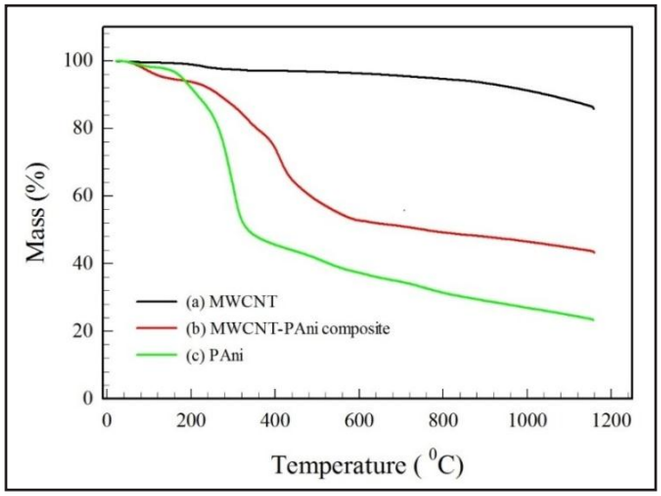

Fig. 5: Thermograms for (a) MWCNT, (b) MWCNT-PAni Composite, and (c) PAni Under Nitrogen Atmosphere

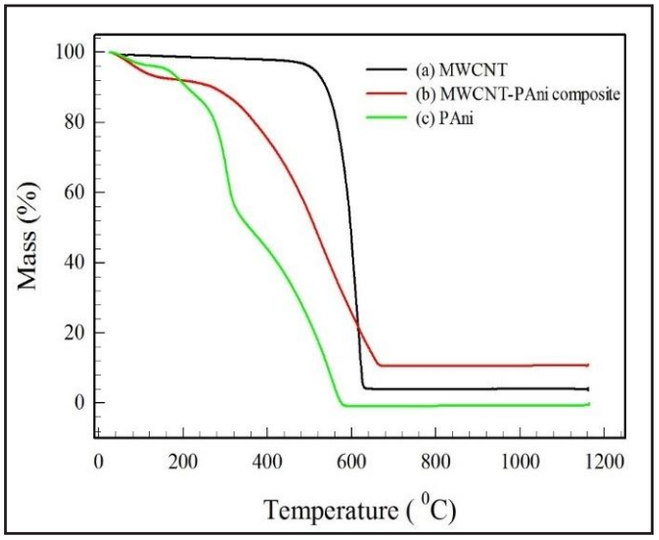

Fig. 6: Thermograms for (a) MWCNT, (b) MWCNT-PAni Composite, and (c) PAni Under Oxygen Atmosphere

e. *Particle Size Analysis*

Size distributions of the particles of MWCNT, MWCNT-PAni composite, and PAni were determined using a particle size analyzer, which measured the solvodynamic diameter of the particles dispersed in dimethyl sulfoxide (DMSO) as shown in Fig. 7. All of the samples consisted of aggregates of particles having a wide variety of sizes, i.e., the particles were highly polydispersed. MWCNTs consisted of aggregates having an average size of ~480 nm (Fig. 7a), while the MWCNT-PAni composite aggregates had an average size of ~434 nm (Fig. 7b).

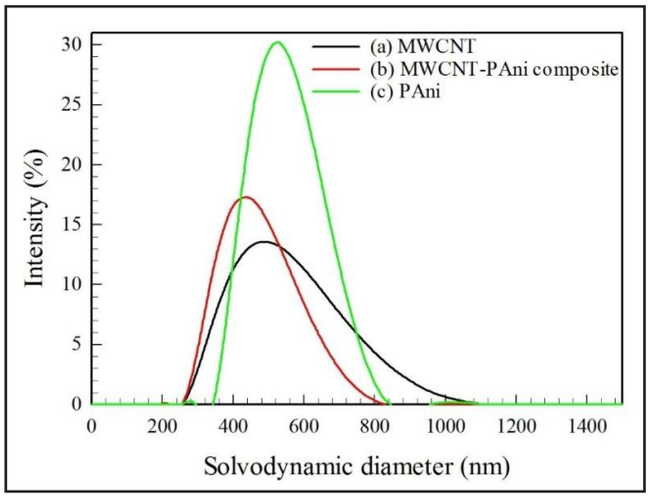

Fig. 7: Particle Size Distribution of (a) MWCNT, (b) MWCNT-PAni Composite, and (c) PAni Dispersed in DMSO

Aggregates of PAni had an average size of ~525 nm (Fig. 7c). MWCNTs, owing to the strong attractive forces between the individual tubes due to van der Waals forces and π-π stacking, formed bundles in their native state, which gave rise to agglomerates of size about ~0.5 μm. The same is true for PAni and MWCNT-PAni composite. These formed aggregates of similar size ranges of the MWCNTs due to strong intermolecular forces of attraction. Due to the tendency of MWCNTs to form aggregates or bundles, the non-covalent dispersion imparted to them by PSS molecules enables the bundles to disintegrate and the individual tubes to get isolated from one another, thus allowing the uniform coating of PAni around the MWCNTs.

f. *Surface Area and Pore Size Distribution Analysis*

Adsorption isotherms for MWCNT, MWCNT-PAni composite, and PAni are shown in Fig. 8. It can be observed that the isotherm for MWCNTs (Fig. 8a) resembles Type-III, indicative of macroporous or a non-porous surface, in spite of MWCNTs adsorbing the greatest volume of gas. In the adsorption isotherm of PAni (Fig. 8c), a hysteresis loop can be seen, corresponding to Type-V [51], from which it can be inferred that the surface is mesoporous and has weak affinity for the adsorbate. The adsorption isotherm of MWCNT-PAni composite (Fig. 8b) represents Type-IV [51], indicating a mesoporous surface on which capillary condensation occurs. Thus, we can conclude that the macropores in the MWCNT structure are changed to mesopores on encapsulating it with PAni, rendering a better

contact area for the percolation of electrolyte when the composite is used as electroactive material on graphite electrode surface.

From BET plots of the samples, the specific surface areas were calculated using the BET equation [52] as tabulated in Table I. The pore volumes and mean pore sizes of the samples derived from their Barrett-Joyner-Halenda (BJH) plots (Fig. 9) are also summarized in Table I. MWCNTs have the largest surface area, while the MWCNT-PAni composite has the least. This suggests that the encapsulation of MWCNTs with PAni reduces its surface area. In addition, since the macropores are reduced to mesopores, the surface area of the MWCNTs is reduced as a result of formation of composite.

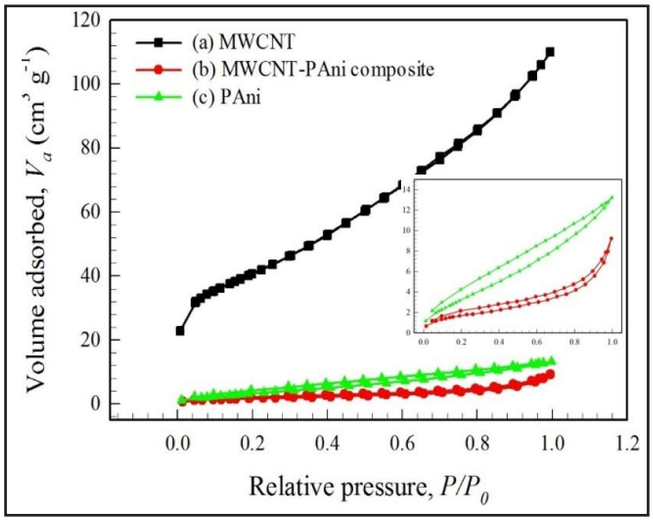

Fig. 8: Nitrogen Adsorption-Desorption Isotherms of (a) MWCNT, (b) MWCNT-PAni Composite, and (c) PAni

The mean pore diameters indicate that all three samples have mesoporous structure. MWCNTs have the highest total pore volume, meaning that a large number of mesopores are present in them which contribute to the macroporous structure, but the MWCNT-PAni composite has the highest mean pore diameter, suggesting a well-defined mesoporous structure, which will facilitate the penetration of electrolyte when the composite is fabricated as a supercapacitor electrode. PAni also has a mesoporous structure and a very low surface area in comparison to MWCNTs.

Table I: Surface Area and Pore Sizes of MWCNT, MWCNT-PAni, Composite, and PAni

Sample	*Specific surface area (m^2 g^{-1})*	*Pore volume (cm^3 g^{-1})*	*Mean pore diameter, r_p (nm)*
MWCNT	143.3	0.17	4.7
MWCNT-PAni composite	6.6	0.01	8.3
PAni	12.2	0.02	6.6

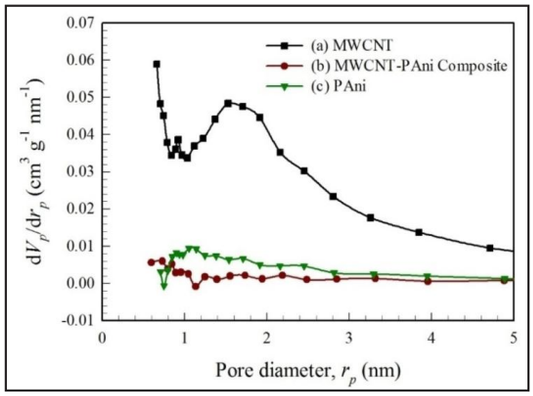

Fig. 9: BJH Plots Showing Pore Size Distribution for (a) MWCNT, (b) MWCNT-PAni Composite, and (c) PAni

B. Model Proposed for the Structure of MWCNT-PAni Composite

In this work, the MWCNTs were dispersed by PSS, which attached themselves to the MWCNTs by van der Waals forces and π-π stacking. Sulfonate groups of PSS are considered to attach to the MWCNTs after their dispersion with PSS.Dong *et al.* [58] proposed the mechanism for such attachment of PAni to CNTs sulfonated with calcium lignosulfonate. In this case, aniline is converted to anilinium ion on addition of dopant, HCl; it then underwent oxidative polymerization to form emeraldine salt of PAni. The probable mechanism for the formation of MWCNT-PAni composite from PSS dispersed MWCNT and doped aniline is illustrated in Fig. 10a. As shown in Fig. 10a, the negatively charged sulfonate groups attached to the MWCNTs acted as templates for the attachment of positively charged anilinium ions, which underwent oxidative polymerization on the MWCNT surface, producing emeraldine salt form which comprised polarons.

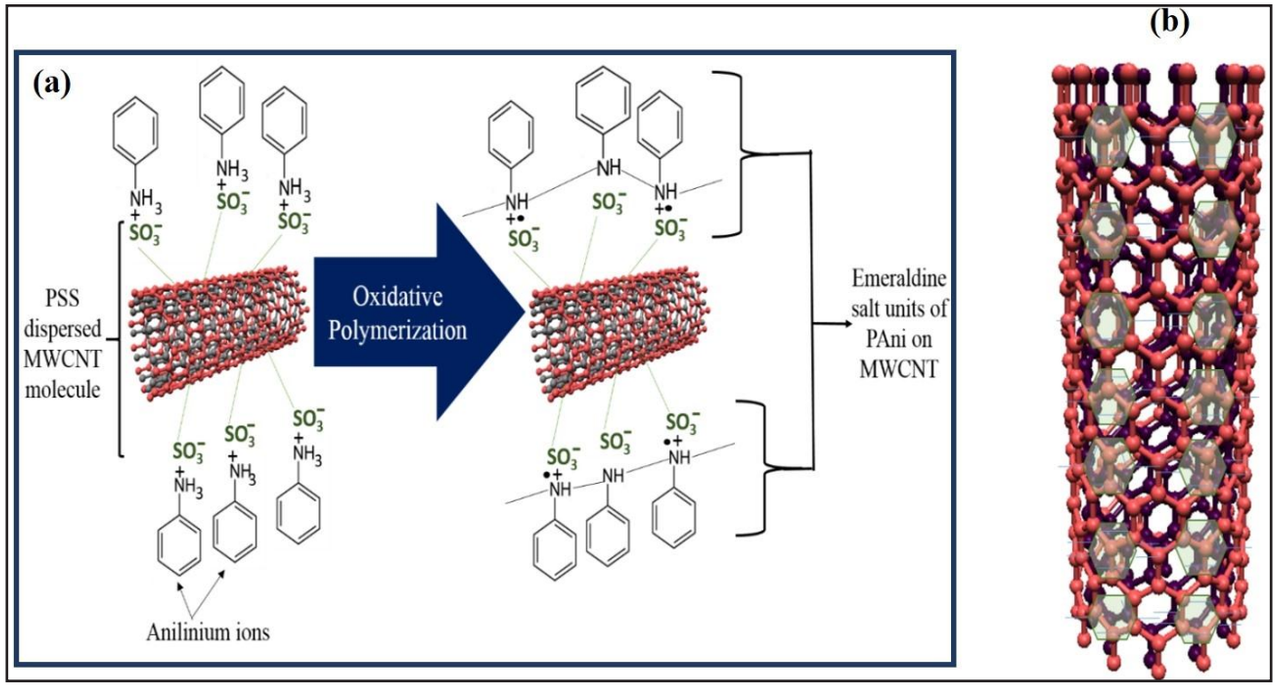

Fig. 10: (a) Schematic Representation the Polymerization of Doped Aniline on PSS Dispersed MWCNTs and (b) MWCNT Encapsulated with Benzenoid and Quinoid Units of PAni

The MWCNTs can thus be visualized to be encapsulated by PAni chains where the benzenoid and quinoid units of which form the aforementioned attractive interactions with the MWCNTs. Similarly, in case of MWCNT-PAni composite, the nanotubes are surrounded by the benzenoid and quinoid units of PAni, as shown in Fig. 10b. Therefore, the decrease in surface area of MWCNTs on encapsulation with PAni as observed with BET and SEM analyses can be explained by this model as the macropores of pristine MWCNTs, after encapsulation, decrease in size, leading to the formation of mesopores in the composite. Such microstructure of the composite would assist to enhance storing capacity of charges of the composite as clarified by capacitance measurement with cyclic voltammetry (vide infra).

C. Electrochemical Characterization

Fig. 11 shows the cyclic voltammograms at scan rates ranging from 5 to 200 mVs^{-1} for the fabricated electrode. The cyclic voltammograms show that within the potential window 0.5 to 1.2 V, the curves have rectangular shape, indicating the absence of Faradaic reactions within this region. The area of the rectangular region (IdV) corresponding to the specific capacitance increases with decreasing potential scan rate.

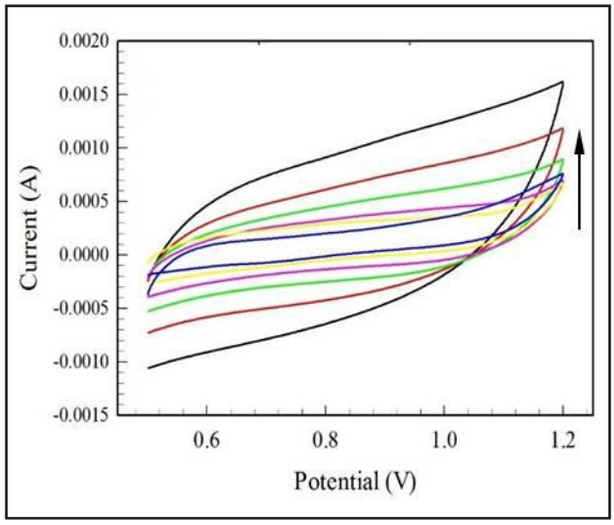

Fig. 11: Cyclic Voltammograms of Graphite Electrode Fabricated with MWCNT-PAni Composite at Scan Rates of 5, 10, 25, 50, 100, and 200 mVs^{-1}. The Direction of the Arrow Indicates Increase in Potential Scan Rate

The variation of specific capacitance, C_s, with scan rate is shown in Fig. 12. Here C_s= IdV/*mv*, where IdV is the area under the region of positive current in the cyclic voltammogram, *m* is the mass of electroactive material in g and *v* is the potential scan rate in Vs^{-1} [53]. The specific capacitance decreases with increase in the potential scan rate. The highest value of C_s, 446 Fg^{-1} was observed at a scan rate of 5 mVs^{-1}, plateauing out at a scan rate of 100 mVs^{-1}. This is due to the fact that the electrolyte ions are only able to reach the outer surface of the electrode at high scan rates, and the electrochemically active material that is accessible only through the deep pores does not actively contribute to the pseudocapacitance [54]. As a result, high scan rates lead to low C_s. The superior capacitive property of this fabricated electrode can be attributed to the nanofibrous morphology of the MWCNT-PAni composite yielding a higher surface area, which enhances the effective access of the electrolyte, and leads to the storage of greater amount of charge via both the double-layer and redox capacitive mechanisms [55].

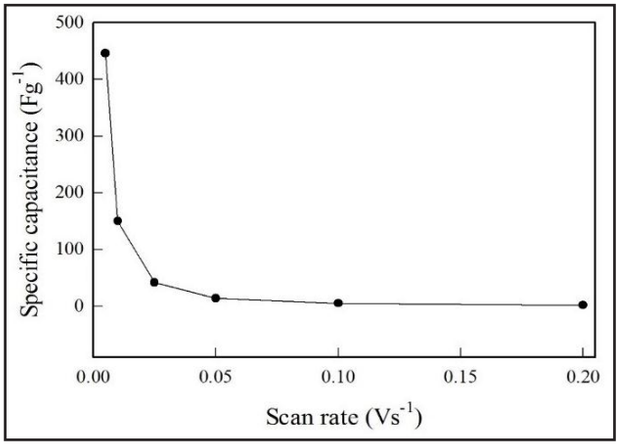

Fig. 12: Variation of Specific Capacitance of the Graphite Electrode Fabricated with MWCNT-PAni Composite as a Function of Potential Scan Rate

The cyclic voltammograms of the fabricated electrode, before and after 800 cycles, at a scan rate of 5 mVs^{-1}, are shown in Fig. 13. The C_s of the electrode after 800 cycles was determined to be 368 Fg^{-1}, which is 82.5% of that before cycling (446 Fg^{-1}), suggesting good retention capability of C_s by the electrode. The slight decrease in specific capacitance upon repeated cycling occurred due to swelling and shrinkage of PAni in the composite, revealing that the mesoporous structure of the composite deteriorates with repeated cycling. It can thus be surmised that increasing the content of MWCNTs in the composite could improve the cycling performance [56].

However, good retention also indicates good interfacial interaction between MWCNTs and PAni, resulting from the highly accessible surface area and low resistivity of the MWCNTs [57], which might have in turn resulted from the superior dispersion of MWCNTs by PSS prior to the synthesis of composite. The mesoporous structure of the composite was additionally involved in the good specific capacitance and retention ability or cycling performance of the composite.

Hence, from the electrochemical data, it can be inferred that MWCNT-PAni composite synthesized by non-covalent dispersion of MWCNTs with polymer wrapping by PSS, when fabricated on a graphite electrode, exhibits superior capacitance behavior in addition to good cycle stability.

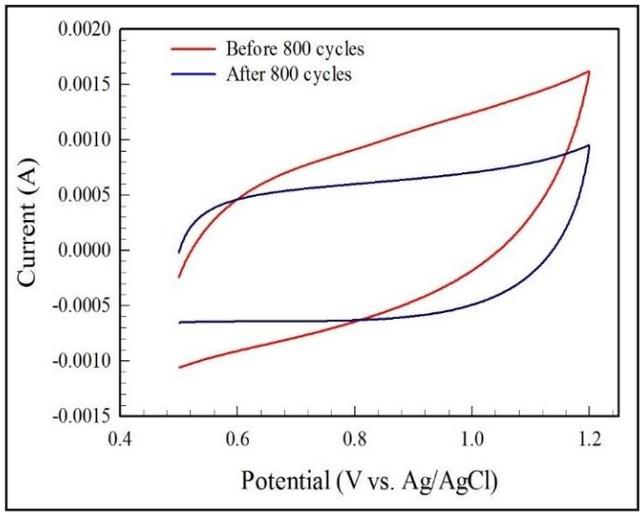

Fig. 13: Cyclic Voltammograms for the Fabricated Electrode at the Scan Rate of 5 mVs^{-1} Before and After 800 Cycles

IV. Conclusions

MWCNTs can be dispersed by an environmentally friendly method of non-covalent functionalization, using a polymer, PSS, prior to synthesizing a composite with PAni to enhance the interfacial interaction between the CNT and PAni. The backbone of PAni is not damaged due to incorporation of MWCNTs in the polymer matrix. Furthermore, the MWCNT-PAni composite has coaxial nanofibrous structure, the average tube diameter of the fibres being of nanodimension, indicating that the MWCNTs, which, in their pristine form, formed dense aggregates or bundles due to strong intermolecular forces of attraction resulting from van der Waals forces and π-π stacking, must have been well dispersed by PSS via static charge repulsion. The incorporation of MWCNTs in the PAni structure also enhances the thermal stability of PAni, in addition to introducing well-defined mesopores in the structure. A hypsochromic shift of the UV-visible absorption peaks for the composite compared to pristine PAni is noticeable due to the presence of strong interactions between the quinoid units of PAni and MWCNTs. Moreover, the MWCNT-PAni composite fabricated working electrode exhibits specific capacitance of 446 Fg^{-1} at a scan rate of 5 mVs^{-1}, which reduces to 82.5% of the initial value after 800 cycles, indicating good cycle stability, and hence holding great potential as a "green" material for application in supercapacitors. The studies also indicate that an increase in the MWCNT mass loading in the composite might increase the cycle stability.

Acknowledgements

The authors acknowledge the support under the subproject, CPSF 231 of the Higher Education Quality Enhancement Project of University Grants Commission of Bangladesh under the Ministry of Education, Government of Bangladesh. The authors also express their gratitude to the Centre for Advanced Research in Sciences of the University of Dhaka, Bangladesh, for allowing the use of its SEM facilities.

References

[1] S. Iijima, "Helical microtubules of graphitic carbon," *Nature,* vol. 354, pp. 56-58, 1991.

[2] P. J. Harris, *Carbon Nanotube Science: Synthesis, Properties and Applications,* Cambridge University Press, p. 301, 2009.

[3] H. Pan, J. Li, and Y. P. Feng, "Carbon nanotubes for supercapacitor," *Nanoscale Res. Lett.,* vol. 5, pp. 654-668, 2010.

[4] M. Campos, and B. Bello Jr., "Mechanism of conduction in doped polyaniline," *J. Phys. D: Appl. Phys.,* vol. 30, pp. 1531-1535, 1997.

[5] S. J. Tang, A. T. Wang, S. Y. Lin, K. Y. Huang, C. C. Yang, J. M. Yeh, and K. C. Chiu, "Polymerization of aniline under various concentrations of APS and HCl," *Polym. J.,* vol. 43, pp. 667-675, 2011.

[6] W. Lu, and L. Dai, "Carbon Nanotube Supercapacitors," In: *Carbon Nanotubes* (ed. J. M. Marulanda) pp. 563-589, INTECH Open Access Publisher, 2010.

[7] Y. K. Zhou, B. L. He, W. J. Zhou, J. Huang, X. H. Li, B. Wu, and H. L. Li, "Electrochemical capacitance of well-coated single-walled carbon nanotube with polyaniline composites," *Electrochim. Acta,* vol. 49, pp. 257-262, 2004.

[8] V. Gupta, and N. Miura, "Polyaniline/single-wall carbon nanotube (PANI/SWCNT) composites for high performance supercapacitors," *Electrochim. Acta,* vol. 52, pp. 1721-1726, 2006.

[9] H. Zhang, G. Cao, Z. Wang, Y. Yang, Z. Shi, and Z. Gu, "Tube-covering-tube nanostructured polyaniline/carbon nanotube array composite electrode with high capacitance and superior rate performance as well as good cycling stability," *Electrochem. Commun.,* vol. 10, pp. 1056-1059, 2008.

[10] Y. Zhou, Z. Y. Qin, L. Li, Y. Zhang, Y. L. Wei, L. F. Wang, and M. F. Zhu, "Polyaniline/multi-walled carbon nanotube composites with core-shell structures as supercapacitor electrode materials," *Electrochim Acta,* vol. 55, pp. 3904-3908, 2010.

[11] M. Hughes, M. S. P. Shaffer, A. C. Renouf, C. Singh, G. Z. Chen, D. J. Fray, and A. H. Windle, "Electrochemical capacitance of nanocomposite films formed by coating aligned arrays of carbon nanotubes with polypyrrole," *Adv. Mater.,* vol. 14, pp. 382-385, 2002.

[12] M. Hughes, G. Z. Chen, M. S. P. Shaffer, D. J. Fray, and A. H. Windle, "Electrochemical capacitance of a nanoporous composite of carbon nanotubes and polypyrrole," *Chem. Mater.,* vol. 14, pp. 1610-1613, 2002.

[13] J. Wang, Y. Xu, X. Chen, and X. Sun, "Capacitance properties of single wall carbon nanotube/polypyrrole composite films," *Compos. Sci. Technol.,* vol. 67, pp. 2981-2985, 2007.

[14] K. H. An, K. K. Jeon, J. K. Heo, S. C. Lim, D. J. Bae, and Y. H. Lee, "High-capacitance supercapacitor using a nanocomposite electrode of single-walled carbon nanotube and polypyrrole," *J. Electrochem. Soc.,* vol. 149, pp. A1058-A1062, 2002.

[15] E. Frackowiak, and F. Be´guin, "Carbon materials for the electrochemical storage of energy in capacitors," *Carbon,* vol. 39, pp. 937-950, 2001.

[16] D. Bélanger, X. Ren, J. Davey, F. Uribe, and S. Gottesfeld, "Characterization and long-term performance of polyaniline-based electrochemical capacitors," *J. Electrochem. Soc.,* vol. 147, pp. 2923-2929, 2000.

[17] F. Fusalba, P. Gouérec, D. Villers, and D. Bélanger, "Electrochemical characterization of polyaniline in nonaqueous electrolyte and its evaluation as electrode material for electrochemical supercapacitors," *J. Electrochem. Soc.,* vol. 148, pp. A1-A6, 2001.

[18] Y. Liu, T. Cui, and K. Varahramyan, "Fabrication and characteristics of polymeric thin-film capacitor," *Solid-State Electron.,* vol. 47, pp. 811-814, 2003.

[19] Y. Liu, T. Cui, and K. Varahramyan, "All-polymer capacitor fabricated with inkjet printing technique," *Solid-State Electron.,* vol. 47, pp. 1543-1548, 2003.

[20] B. C. Kim, J. M. Ko, and G. G. Wallace, "A novel capacitor material based on Nafion-doped polypyrrole," *J. Power Sources,* vol. 177, pp. 665-668, 2008.

[21] K. C. Liu, and M. A. Anderson, "Porous nickel oxide/nickel films for electrochemical capacitors," *J. Electrochem. Soc.,* vol. 143, pp. 124-130, 1996.

[22] V. Srinivasan, and J. W. Weidner, "An electrochemical route for making porous nickel oxide electrochemical capacitors," *J. Electrochem. Soc.,* vol. 144, pp. L210-L213, 1997.

[23] M. S. Wu, and P. C. J. Chiang, "Fabrication of nanostructured manganese oxide electrodes for electrochemical capacitors," *Electrochem. Solid-State Lett.,* vol. 7, pp. A123-A126, 2004.

[24] M. S. Wu, Y. A. Huang, C. H. Yang, and J. J. Jow, "Electrodeposition of nanoporous nickel oxide film for

electrochemical capacitors," *Int. J. Hydrogen Energy,* vol. 32, pp. 4153-4159, 2007.

[25] X. Lang, A. Hirata, T. Fujita, and M. Chen, "Nanoporous metal/oxide hybrid electrodes for electrochemical supercapacitors," *Nature Nanotech.,* vol. 6, pp. 232-236, 2011.

[26] L. Chen, L. J. Sun, F. Luan, Y. Liang, Y. Li, and X. X. Liu, "Synthesis and pseudocapacitive studies of composite films of polyaniline and manganese oxide nanoparticles," *J. Power Sources,* vol. 195, pp. 3742-3747, 2010.

[27] X. Li, H. Zhang, G. Wang and Z. Jiang, "A novel electrode material based on a highly homogeneous polyaniline/titanium oxide hybrid for high-rate electrochemical capacitors," *J. Mater. Chem.,* vol. 20, pp. 10598-10601, 2010.

[28] B. X. Zou, Y. Liang, X. X. Liu, D. Diamond, and K. T. Lau, "Electrodeposition and pseudocapacitive properties of tungsten oxide/polyaniline composite," *J. Power Sources,* vol. 196, pp. 4842-4848, 2011.

[29] J. G. Wang, Y. Yang, Z. H. Huang, and F. Kang, "Interfacial synthesis of mesoporous MnO_2/polyaniline hollow spheres and their application in electrochemical capacitors," *J. Power Sources,* vol. 204, pp. 236-243, 2012.

[30] T. Osaka, X. Liu, M. Nojima, and T. Momma, "An electrochemical double layer capacitor using an activated carbon electrode with gel electrolyte binder," *J. Electrochem. Soc.,* vol. 146, pp. 1724-1729, 1999.

[31] K. Okajima, A. Ikeda, K. Kamoshita, and M. Sudoh, "High rate performance of highly dispersed C_{60} on activated carbon capacitor," *Electrochim. Acta,* vol. 51, pp. 972-977, 2005.

[32] C. Niu, E. K. Sichel, R. Hoch, D. Moy, and H. Tennent, "High power electrochemical capacitors based on carbon nanotube electrodes," *Appl. Phys. Lett.,* vol. 70, pp. 1480-1482, 1997.

[33] B. Zhang, J. Liang, C. L. Xu, B. Q. Wei, D. B. Ruan, and D. H. Wu, "Electric double-layer capacitors using carbon nanotube electrodes and organic electrolyte," *Mater. Lett.,* vol. 51, pp. 539-542, 2001.

[34] J. H. Chen, W. Z. Li, D. Z. Wang, S. X. Yang, J. G. Wen, and Z. F. Ren, "Electrochemical characterization of carbon nanotubes as electrode in electrochemical double-layer capacitors," *Carbon,* vol. 40, pp. 1193-1197, 2002.

[35] C. Du, and N. Pan, "High power density supercapacitor electrodes of carbon nanotube films by electrophoretic deposition," *Nanotechnology,* vol. 17, pp. 5314-5318, 2006.

[36] W. Lu, L. Qu, K. Henry, and L. Dai, "High performance electrochemical capacitors from aligned carbon nanotube electrodes and ionic liquid electrolytes," *J. Power Sources,* vol. 189, pp. 1270-1277, 2009.

[37] D. Yu, and L. Dai, "Self-assembled graphene/carbon nanotube hybrid films for supercapacitors," *J. Phys. Chem. Lett.,* vol. 1, pp. 467-470, 2010.

[38] P. C. Ma, N. A. Siddiqui, G. Marom, and J. K. Kim, "Dispersion and functionalization of carbon nanotubes for polymer-based nanocomposites: A review," *Composites: Part A,* vol. 41, pp. 1345-1367, 2010.

[39] B. McCarthy, J. N. Coleman, R. Czerw, A. B. Dalton, D. L. Carroll, and W. J. Blau, "Microscopy studies of nanotube-conjugated polymer interactions," *Synth. Met.,* vol. 121, pp. 1225-1226, 2001.

[40] D. E. Hill, Y. Lin, A. M. Rao, L. F. Allard, and Y. P. Sun, "Functionalization of carbon nanotubes with polystyrene," *Macromolecules,* vol. 35, pp. 9466-9471, 2002.

[41] X. Gong, J. Liu, S. Baskaran, R. D. Voise, and J. S. Young, "Surfactant-assisted processing of carbon nanotube/polymer composites," *Chem. Mater.,* vol. 12, pp. 1049-1052, 2002.

[42] S. Cui, R. Canet, A. Derre, M. Couzi, and P. Delhaes, "Characterization of multiwall carbon nanotubes and influence of surfactant in the nanocomposite processing," *Carbon,* vol. 41, pp. 797-809, 2003.

[43] L. Vaisman, G. Marom, and H. D. Wagner, "Dispersions of surface-modified carbon nanotubes in water-soluble and water-insoluble polymers," *Adv. Funct. Mater.,* vol. 16, pp. 357-363, 2006.

[44] Y. Geng, M. Y. Liu, J. Li, X. M. Shi, and J. K. Kim, "Effects of surfactant treatment on mechanical and electrical properties of CNT/epoxy nanocomposites," *Composites: Part A,* vol. 39, pp. 1876-1883, 2008.

[45] Q. Li, J. Liu, J. Zou, A. Chunder, Y. Chen, and L. Zhai, "Synthesis and electrochemical performance of multiwalled carbon nanotube/polyaniline/MnO_2 ternary coaxial nanostructures for supercapacitors," *J. Power Sources,* vol. 196, pp. 565-572, 2011.

[46] X. Zhang, J. Zhang, and Z. Liu, "Tubular composite of doped polyaniline with multi-walled carbon nanotubes," *Appl. Phys. A,* vol. 80, pp. 1813-1817, 2005.

[47] K. R. Reddy, B. C. Sin, C. H. Yoo, D. Sohn, and Y. Lee, "Coating of multiwalled carbon nanotubes with polymer nanospheres through microemulsion polymerization," *J. Colloid Interface Sci.,* vol. 340, pp. 160-165, 2009.

[48] Y. Yu, B. Che, Z. Si, L. Li, W. Chen, and G. Xue, "Carbon nanotube/polyaniline core-shell nanowires prepared by in situ inverse microemulsion," *Synthetic Met.,* vol. 150, pp. 271-277, 2005.

[49] H. Guo, H. Zhu, H. Lin, and J. Zhang, "Synthesis of polyaniline/multi-walled carbon nanotube nanocomposites in water/oil microemulsion," *Mater. Lett.,* vol. 62, pp. 3919-3921, 2008.

[50] L. Shi, R. P. Liang, and J. D. Qiu, "Controllable deposition of platinum nanoparticles on polyaniline-functionalized carbon nanotubes," *J. Mater. Chem.,* vol. 22, pp. 17196-17203, 2012.

[51] P. B. Balbuena, and K. E. Gubbins, "Theoretical interpretation of adsorption behavior of simple fluids in slit pores," *Langmuir,* vol. 9, pp. 1801-1814, 1993.

[52] S. Brunauer, P. H. Emmett, and E. Teller, "Adsorption of gases in multimolecular layers," *J. Am. Chem. Soc.,* vol. 60, pp. 309-319, 1938.

[53] H. Jiang, L. Yang, C. Li, C. Yan, P. S. Lee, and J. Ma, "High–rate electrochemical capacitors from highly graphitic carbon–tipped manganese oxide/mesoporous carbon/manganese oxide hybrid nanowires," *Energy Environ. Sci.,* vol. 4, pp. 1813-1819, 2011.

[54] R. K. Sharma, and L. Zhai, "Multiwall carbon nanotube supported poly (3, 4-ethylenedioxythiophene)/manganese oxide nano-composite electrode for super-capacitors," *Electrochim. Acta,* vol. 54, pp. 7148-7155, 2009.

[55] S. R. Sivakkumar, W. J. Kim, J. A. Choi, D. R. MacFarlane, M. Forsyth, and D. W. Kim, "Electrochemical performance of polyaniline nanofibres and polyaniline/multiwalled carbon nanotube composite as an electrode material for aqueous redox supercapacitors," *J. Power Sources,* vol. 171, pp. 1062-1068, 2007.

[56] Y. Zhou, Z. Y. Qin, L. Li, Y. Zhang, Y. L. Wei, L. F. Wang, and M. F. Zhu, "Polyaniline/multi-walled carbon nanotube composites with core-shell structures as supercapacitor electrode materials," *Electrochim. Acta,* vol. 55, pp. 3904-3908, 2010.

[57] J. Zhang, L. B. Kong, B. Wang, Y. C. Luo, and L. Kang, "In-situ electrochemical polymerization of multi-walled carbon nanotube/polyaniline composite films for electrochemical supercapacitors," *Synthetic Met.,* vol. 159, pp. 260-266, 2009.

[58] J. Q. Dong, and Q. Shen, "Enhancement in solubility and conductivity of polyaniline with lignosulfonate modified carbon nanotube," *J. Polym. Sci. Part B: Polym. Phys.,* vol. 47, pp. 2036-2046, 2009.